



High-Fidelity Three-Dimensional Simulation of the GE90

Mark G. Turner
University of Cincinnati, Cincinnati, Ohio

Andrew Norris
Ohio Aerospace Institute, Brook Park, Ohio

Joseph P. Veres
Glenn Research Center, Cleveland, Ohio

The NASA STI Program Office . . . in Profile

Since its founding, NASA has been dedicated to the advancement of aeronautics and space science. The NASA Scientific and Technical Information (STI) Program Office plays a key part in helping NASA maintain this important role.

The NASA STI Program Office is operated by Langley Research Center, the Lead Center for NASA's scientific and technical information. The NASA STI Program Office provides access to the NASA STI Database, the largest collection of aeronautical and space science STI in the world. The Program Office is also NASA's institutional mechanism for disseminating the results of its research and development activities. These results are published by NASA in the NASA STI Report Series, which includes the following report types:

- **TECHNICAL PUBLICATION.** Reports of completed research or a major significant phase of research that present the results of NASA programs and include extensive data or theoretical analysis. Includes compilations of significant scientific and technical data and information deemed to be of continuing reference value. NASA's counterpart of peer-reviewed formal professional papers but has less stringent limitations on manuscript length and extent of graphic presentations.
- **TECHNICAL MEMORANDUM.** Scientific and technical findings that are preliminary or of specialized interest, e.g., quick release reports, working papers, and bibliographies that contain minimal annotation. Does not contain extensive analysis.
- **CONTRACTOR REPORT.** Scientific and technical findings by NASA-sponsored contractors and grantees.

- **CONFERENCE PUBLICATION.** Collected papers from scientific and technical conferences, symposia, seminars, or other meetings sponsored or cosponsored by NASA.
- **SPECIAL PUBLICATION.** Scientific, technical, or historical information from NASA programs, projects, and missions, often concerned with subjects having substantial public interest.
- **TECHNICAL TRANSLATION.** English-language translations of foreign scientific and technical material pertinent to NASA's mission.

Specialized services that complement the STI Program Office's diverse offerings include creating custom thesauri, building customized databases, organizing and publishing research results . . . even providing videos.

For more information about the NASA STI Program Office, see the following:

- Access the NASA STI Program Home Page at <http://www.sti.nasa.gov>
- E-mail your question via the Internet to help@sti.nasa.gov
- Fax your question to the NASA Access Help Desk at 301-621-0134
- Telephone the NASA Access Help Desk at 301-621-0390
- Write to:
NASA Access Help Desk
NASA Center for Aerospace Information
7121 Standard Drive
Hanover, MD 21076



High-Fidelity Three-Dimensional Simulation of the GE90

Mark G. Turner
University of Cincinnati, Cincinnati, Ohio

Andrew Norris
Ohio Aerospace Institute, Brook Park, Ohio

Joseph P. Veres
Glenn Research Center, Cleveland, Ohio

Prepared for the
16th Computational Fluid Dynamics Conference and
the 33rd Fluid Dynamics Conference and Exhibit
sponsored by the American Institute of Aeronautics and Astronautics
Orlando, Florida, June 23–26, 2003

National Aeronautics and
Space Administration

Glenn Research Center

Acknowledgments

The authors wish to thank the support received from the Aerospace Propulsion and Power Program at NASA Glenn Research Center under the Vehicle Systems Program and Office of Aerospace Technology. The authors also appreciate the continued interest by GE Aircraft Engines in the simulation of the GE90.

This report is a formal draft or working paper, intended to solicit comments and ideas from a technical peer group.

Trade names or manufacturers' names are used in this report for identification only. This usage does not constitute an official endorsement, either expressed or implied, by the National Aeronautics and Space Administration.

This work was sponsored by the Low Emissions Alternative Power Project of the Vehicle Systems Program at the NASA Glenn Research Center.

Available from

NASA Center for Aerospace Information
7121 Standard Drive
Hanover, MD 21076

National Technical Information Service
5285 Port Royal Road
Springfield, VA 22100

Available electronically at <http://gltrs.grc.nasa.gov>

High-Fidelity Three-Dimensional Simulation of the GE90

Mark G. Turner
University of Cincinnati
Cincinnati, Ohio 45220

Andrew Norris
Ohio Aerospace Institute
Brook Park, Ohio 44142

Joseph P. Veres
National Aeronautics and Space Administration
Glenn Research Center
Cleveland, Ohio 44135

Summary

A full-engine simulation of the three-dimensional flow in the GE90-94B high bypass ratio turbofan engine has been achieved. It would take less than 11 hr of wall clock time if starting from scratch through the exploitation of parallel processing. The simulation of the compressor components, the cooled high-pressure turbine, and the low-pressure turbine was performed using the APNASA turbomachinery flow code. The combustor flow and chemistry were simulated using the National Combustor Code (NCC). The engine simulation matches the engine thermodynamic cycle for a sea-level takeoff condition. The simulation is started at the inlet of the fan and progresses downstream. Comparisons with the cycle point are presented. A detailed look at the blockage in the turbomachinery is presented as one measure to assess and view the solution and the multistage interaction effects.

Introduction

One of the goals of the Numerical Propulsion System Simulation (NPSS) Program at the NASA Glenn Research Center has been to demonstrate a high-fidelity three-dimensional turbofan engine simulation. This simulation will support the multidimensional, multifidelity, multidiscipline concept of the design and analysis of propulsion systems for the future. This paper describes the

current status of one major part of that goal: the complete turbofan engine simulation using an advanced three-dimensional Navier-Stokes turbomachinery solver, APNASA, coupled with the National Combustion Code (NCC).

A production engine has been chosen for this demonstration: the GE90 turbofan engine shown in figure 1. A sea-level, Mach 0.25, takeoff condition has been used for the simulation. The main reason is that detailed cooling flows for the turbine are well known at takeoff since this represents the cooled turbine design condition. Since the cooling flow represents a significant amount of the required boundary condition information, it was felt this was a good point for the simulation. It also represents a condition where there are the highest temperatures and most stress in the engine, and is therefore a practical point to gain further understanding.

The GE90 development program included component testing of all the turbomachinery as well as the combustor. The full engine simulation effort has taken advantage of this. All the turbomachinery components have been analyzed and compared to component test data to validate and calibrate the approach. These efforts have been presented by Adamczyk (ref. 2), Turner et al. (ref. 11), and Turner (ref. 12). Also presented by Turner et al. (ref. 11) was the coupled high- and low-pressure turbine run at engine conditions. Turner (ref. 13) has presented an uncoupled fan and booster with a coupled high-pressure compressor (HPC) combustor, high-pressure turbine (HPT), and low-pressure turbine (LPT). This



Figure 1.—GE90 turbofan engine.

paper expands on that work by coupling all the components.

One other important aspect of this effort is to reduce the wall clock time to obtain a simulation by exploiting parallel processing as much as possible. Reduced solution times are necessary to efficiently explore the physics of a problem, to validate a code, and most importantly, to impact design.

The approach used is presented in the next section of this paper that describes the GE90 engine, the turbomachinery solver, the combustor solver, and the coupling strategy. The aerodynamic blockage is derived which is a catchall for three-dimensional and multistage effects. It is a useful quantity for assessing and visualizing the solution. The results section briefly discusses the simulation compared with the cycle, the solution timings, and the aerodynamic blockage effects.

Symbols

A	annular area
h	enthalpy
P	pressure
r	radius
R	gas constant
T	temperature
V	velocity
\dot{m}	mass flow rate
ρ	density
ω	shaft rotational speed
γ	specific heat ratio

Subscripts and superscripts:

h	hub
t	tip
T	total or stagnation conditions

θ	tangential
z	axial
$\bar{\bar{\quad}}$	mass-averaged
$\bar{\quad}$	mass-averaged
$\underline{\quad}$	derived quantity

Approach

The overall approach is to simulate the turbomachinery components using the APNASA code that incorporates the average passage model. The compression system is currently broken into three domains: the fan, booster, and HPC. Profiles are passed from one of these domains to the next. Both the HPT and LPT are simulated in one domain. The combustion simulation uses the parallel, unstructured code (NCC). Coupling between these codes is across common interface planes.

The GE90 Turbofan Engine

The GE90-94B is a production engine offered on the Boeing 777-200ER as shown in a cutaway schematic in figure 1. It is a 94 000 lb thrust version of the GE90 with a bypass ratio of 8.4. The fan is 120 in. in diameter comprising 22 composite wide-chord blades. The fan outlet guide vane (OGV) has several types with different camber to guide the bypass flow around the pylon. Only the nominal type is modeled in this simulation.

The booster, or low-pressure compressor, consists of three stages and rotates on a common shaft with the fan and LPT. The three stages comprise seven blade rows. A fan frame strut separates the booster from the HPC. The 10-stage HPC has a 23 to 1 pressure ratio and has been redesigned using three-dimensional aerodynamic (3-D Aero) technology. The original GE90 HPC was a scale of the HPC developed for the NASA/GE Energy Efficient Engine (E³) program. The HPC is on a common shaft with the HPT.

The combustor is a dual dome annular design for reduced NO_x emission levels and reduced unburned hydrocarbon, carbon monoxide, and smoke levels. There are 30 pairs of fuel nozzles around the annulus.

The HPT has two stages comprising four blade rows. There is a turbine midframe strut separating the HPT and LPT. It diffuses the flow through a

high-angle outer diameter casing to a high diameter for an improved efficiency LPT. The LPT has 6 stages comprising 12 blade rows. A turbine rear frame strut follows this.

The simulation consists of 49 blade rows of turbomachinery and a 24° sector of the combustor. The 49 blade rows include the fan, bypass splitter, nominal OGV (the pylon and different OGV types are not modeled), the 3-stage booster (7 blade rows), the fan frame strut, the 10-stage HPC (21 blade rows), the 2-stage HPT (4 blade rows), the turbine midframe strut, the 6-stage LPT (12 blade rows), and the turbine rear frame strut. Although there are 30 pairs of fuel nozzles, actual periodicity of the geometry requires the modeling of two pairs of fuel nozzles, or a 24° sector. Unique cooling arrangements make one pair of fuel nozzles a-periodic.

Turbomachinery Simulation

The average passage approach is incorporated in the code APNASA as discussed by Adamczyk et al. (ref. 1). Adamczyk (ref. 2) in another paper also discusses the use of this tool to support turbomachinery aerodynamic design. Kirtley et al. (ref. 5) generalized the closure and allowed grids with less shear to be used. Some of the numerical details used in APNASA are

1. Four-stage Runge-Kutta explicit three-dimensional RANS solver
2. Local time steps
3. Implicit residual smoothing
4. Implicit k - ϵ turbulence model
5. Two levels of parallel using MPI message passing

Some of the physical models APNASA can handle are

1. Multistage effects modeled using the average passage formulation of Adamczyk and generalized for nonpure H-grids
2. Wall functions
3. Rotor tip clearance flow
4. Compressor bleed, stator leakage, and turbine cooling flow through inflow and outflow leakage boundary conditions or source terms

5. Stator button geometry
6. Real gas effects with a linear relation between the ratio of specific heats and temperature
7. Flow-path modifications directed by work of Hunter (ref. 4) to simulate cavities

All turbomachinery components have been simulated at engine conditions.

The HPC simulation in this full engine simulation builds on the HPC component simulation presented by Adamczyk (ref. 2). To match the thermodynamic cycle model of the HPC, APNASA was run by adjusting the inlet total pressure to match the exit corrected mass flow. The turbine simulation is identical to that presented by Turner et al. (ref. 10) except that the combustor profiles have been used as a boundary condition and the shaft speeds were set to the cycle values. The corrected and physical shaft rotational speeds were held constant at cycle values.

Combustor Simulation

The combustor has been simulated using the NCC explained by Ebrahimi et al. (ref. 3), Liu (ref. 6), and Ryder and McDivitt (ref. 8). This is a parallel-unstructured solver that uses a preconditioner to efficiently handle low Mach number flows. The Navier-Stokes flow solver is based on an explicit four-stage Runge-Kutta scheme. Turbulence closure is obtained via the standard k - ϵ model with a high Reynolds number wall function or a nonlinear k - ϵ model for swirling flows. The solver can be linked to any computer-aided design system via the Patran file system. CAD geometry can then be imported into the NCC system relatively easily.

The NCC can be run with a gaseous fuel or by modeling the spray combustion process. Gaseous fuel with finite-rate chemistry has been used in the simulations thus far.

Coupling

The coupling between APNASA and NCC takes place at an interface plane. There are many issues to address when coupling codes that are very different, and even have different models for properties. Several key quantities must be

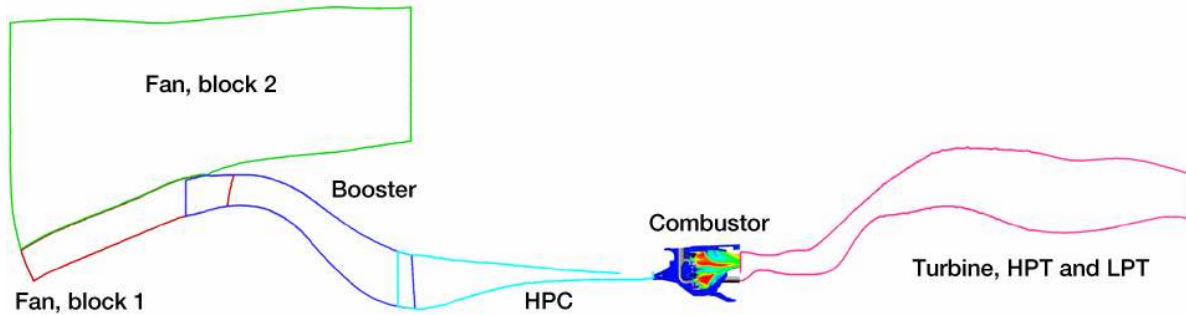


Figure 2.—Five domains simulated in sequence inlet to exit.

conserved from one code to the next. The mass flow must be conserved and is the most critical. The next most important quantity to conserve is the mass averaged total enthalpy. Since mass flow is conserved, this guarantees the total enthalpy flux is also conserved. For turbomachinery applications, the next important conserved quantity is the angular momentum. After this, the total pressure is conserved, and finally the profiles of these quantities. Turner et al. (ref. 13) have presented details of this coupling.

Figure 2 shows the five domains simulated. Each component had been run near the cycle condition, and matched fairly well. The simulation is then run sequentially with the fan first, followed by the booster, HPC, combustor, and turbine. Scripts on the Origin 3000 at NASA Ames have been written so the downstream domain boundary condition is set up and the downstream component is submitted to the batch queue automatically after the solution of the current domain has completed.

Blockage Analysis

Blockage is derived as a way to integrate overall three-dimensional effects in the tangential direction. It is often a quantity used as a catchall for analyzing experimental results when trying to match continuity and using measured flow angles, total temperature, and total and static pressure. Adamczyk (ref. 2) presented some spanwise integrated blockage calculations just downstream of blade row trailing edges for the GE90 compressor. Turner et al. (ref. 13) have presented the blockage for the GE90 turbine. The following analysis differs from those definitions of blockage in that the mass-averaged total pressure has been used instead of the momentum-averaged total pressure. This

was done because a mass average has somewhat more meaning in a turbine. Also the radial flow angle uses the area averaged axial and radial fluxes rather than finding the radial angle that would have zero normal momentum flux. This was done for convenience of the calculation.

The following are defined at each spanwise grid-face of an axisymmetric grid by integrating the flow field: the mass-averaged values of total pressure ($\overline{P_T}$), total enthalpy ($\overline{h_T}$), and angular momentum ($\overline{rV_\theta}$). The mass flow rate (\dot{m}) evaluated by integrating in the tangential direction and the area projections in the axial and radial direction (A_z and A_r) are also needed. The following area averages are also used: radial momentum ($\overline{\rho V_r}$), axial momentum ($A_z \overline{\rho V_z}$), and pressure (\overline{p}). The area averages are obtained using the weights and pointers needed for the closure as described by Kirtley (ref. 5). The mass-averaged quantities use area averages of fluxes. Quantities with an under-bar are derived.

$$\underline{V_\theta} = \frac{\overline{rV_\theta}}{r} \quad (1)$$

$$\underline{\phi} = \tan^{-1} \left(\frac{\overline{\rho V_r}}{\overline{\rho V_z}} \right) \quad (2)$$

$$\underline{V} = \sqrt{\underline{V_z}^2 + \underline{V_r}^2 + \underline{V_\theta}^2} \quad (3)$$

$$\underline{V_r} = \underline{V_z} \tan \underline{\phi} \quad (4)$$

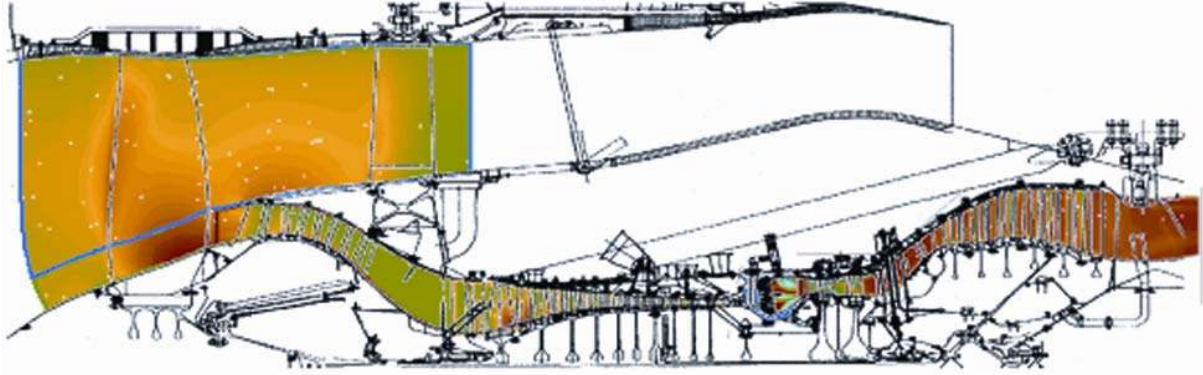


Figure 3.—Schematic of simulation.

From equations (3) and (4), therefore

$$\underline{V}_z = \sqrt{\frac{V^2 - V_\theta^2}{1 + \tan^2 \phi}} \quad (5)$$

The total enthalpy is defined such that

$$\underline{h} = \overline{h_T} - \frac{V^2}{2} \quad (6)$$

\underline{T} and $\underline{T_T}$ are calculated from \underline{h} and $\overline{h_T}$ using the linear function of γ with temperature as described by Turner (ref. 10). An approximation to the isentropic relation using an average $\underline{\gamma}$ yields

$$\frac{\overline{P}}{\overline{P_T}} = \left(\frac{\underline{T}}{\underline{T_T}} \right)^{(\underline{\gamma}/(\underline{\gamma}-1))} \quad (7)$$

Equations (5) to (7) and the relations of $\underline{\gamma}$ on temperature are iterated because of the nonlinear enthalpy-temperature relation. The equation of state is

$$\underline{\rho} = \frac{\overline{P}}{RT} \quad (8)$$

The flow rate is

$$\dot{m} = b_{aero} b_{metal} \underline{\rho} (\underline{V}_z A_z + \underline{V}_r A_r) \quad (9)$$

where b_{metal} is the metal blockage in the tangential direction. The term b_{aero} is the aero blockage and

has been introduced as an overall parameter to represent the three-dimensional effects. Solving for aero blockage yields:

$$b_{aero} = \frac{\dot{m}}{b_{metal} \underline{\rho} (\underline{V}_z A_z + \underline{V}_r A_r)} \quad (10)$$

The derived absolute and relative flow angles can be calculated:

$$\underline{W}_\theta = \underline{V}_\theta - r\omega \quad (11)$$

$$\underline{\alpha} = \tan^{-1} \frac{\underline{V}_\theta}{\underline{V}_z} \quad (12)$$

$$\underline{\beta} = \tan^{-1} \frac{\underline{W}_\theta}{\underline{V}_z} \quad (13)$$

Results

The simulation has fully coupled the fan, booster, HPC, combustor, and the turbines at the sea-level takeoff condition. Figure 3 is a schematic of the overall simulation result showing the axisymmetric solution with an engine cross section superimposed.

Figure 4 shows the geometry of the GE90 combustor, where the dual annular fuel nozzle arrangement can be seen. The high-pressure turbine nozzles can also be seen in this figure, but are not part of this combustor simulation. The unstructured grid used for the combustor simulation is shown in figure 5. Figure 6 shows contours of total pressure and total temperature at a plane cutting through the centerline of each fuel nozzle. The

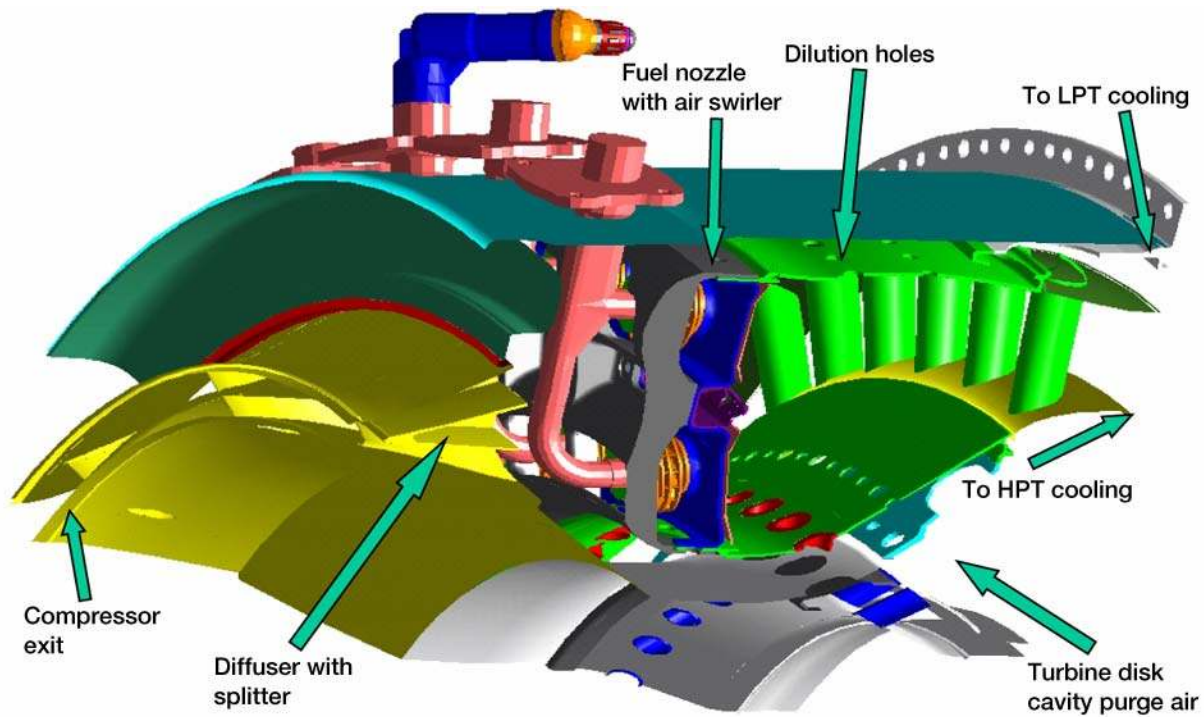


Figure 4.—Geometry of the GE90 Combustor.

Grid generated with FEMAP, adapted grid with NCC solution

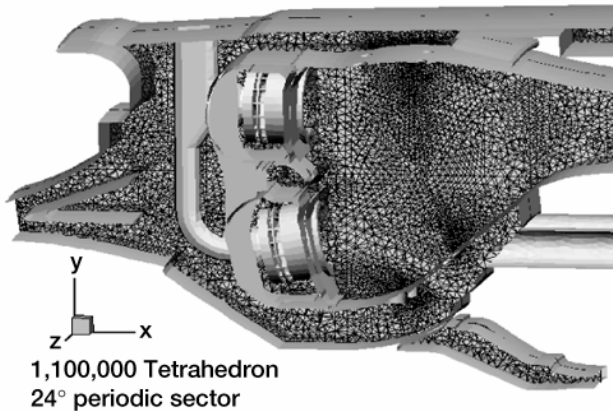


Figure 5.—Unstructured grid of the GE90 combustor used by NCC.

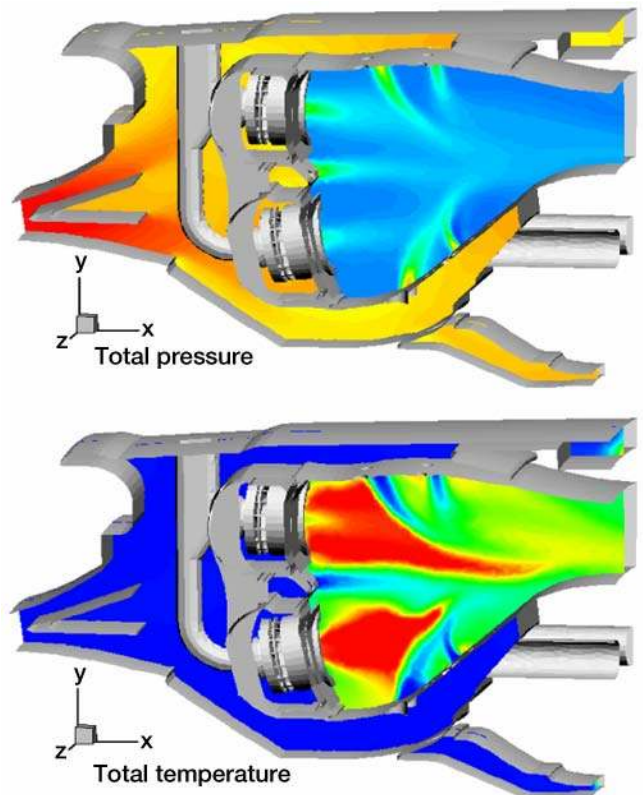


Figure 6.—Combustor simulation.

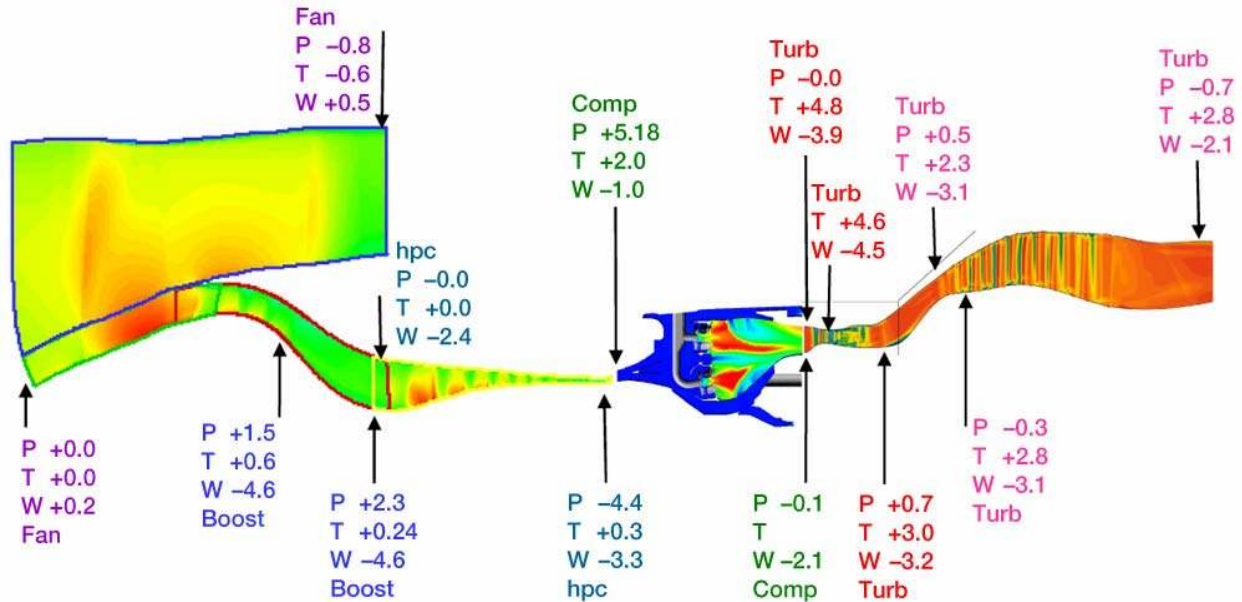


Figure 7.—Full engine simulation comparison to cycle. Percent difference in total pressure (P), total temperature (T), and flow rate (W).

TABLE I.—COMPUTER SIMULATION RUN TIMES.

Component	Number of blade rows	Number of iterations	Number of processors	Wall-clock time	Case from scratch (extrapolated)		
					Number of iterations	Number of processors	Wall-clock time
Fan	3	50	16	0:02:04	8 000	64	1:22:40
Booster	8	6 000	256	1:15:01	6 000	256	1:15:01
HPC	21	10 000	512	1:53:17	10 000	512	1:53:17
Combustor		1 000	256	0:11:07	31 000	256	3:53:00
Turbine	18	10 000	512	1:56:36	10 000	512	1:56:36
Total				5:18:05			10:20:34

dilution jets and their impact are clearly seen. Also seen is the substantial drop in total pressure across the combustor nozzles and liner.

Based on extensive efforts to reduce runtime by exploiting parallel computing, the simulation has been run in just over 5 hr as shown in table I. The fan and combustor did not need to be run very long since they were already at the converged point. A solution from scratch with components near the cycle conditions would take 10 hr and 20 min.

A comparison of the simulation with the cycle is shown in figure 7. Percent difference in total pressure, total temperature, and flow rate are shown. The profile out of the booster has been adjusted to obtain the cycle pressure and temperature at the HPC inlet due to the sensitivity of the full 21-blade HPC simulation. The flow in the

HPC is low as is the pressure ratio. Other discrepancies can also be seen for some of the other components. The problem is that the simulated components cannot duplicate the cycle conditions with the prescribed geometry (including the variable geometry settings). Work is underway to map the components as minimaps so that the cycle can be rerun and be self-consistent with the simulation.

Figure 8 shows the power balance that has been calculated (it is normalized by the fan and booster work). The power from the fan is based on the enthalpy rise, whereas the other components are based on torque from pressure and skin friction. The power to pump the cooling flows has not been subtracted from the HPT work. The work by the HPC has been under predicted which is consistent with the pressure rise.

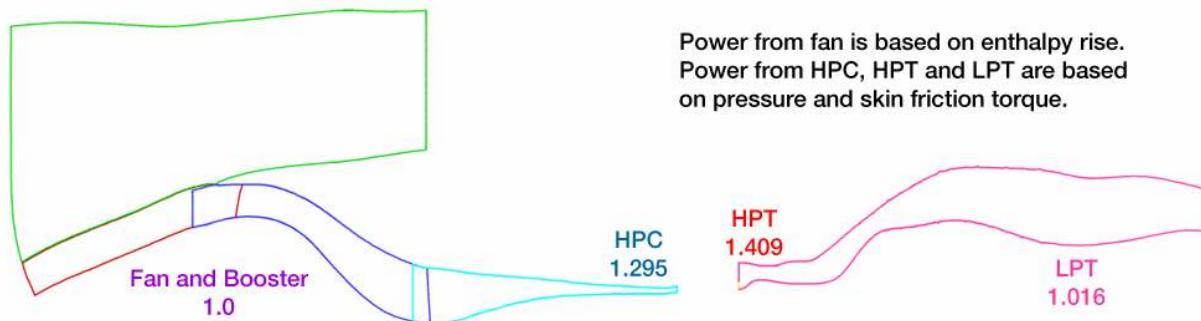


Figure 8.—Power balance (power normalized by fan and booster). Power to pump cooling flows not subtracted from HPT. Work by HPC under-predicted..

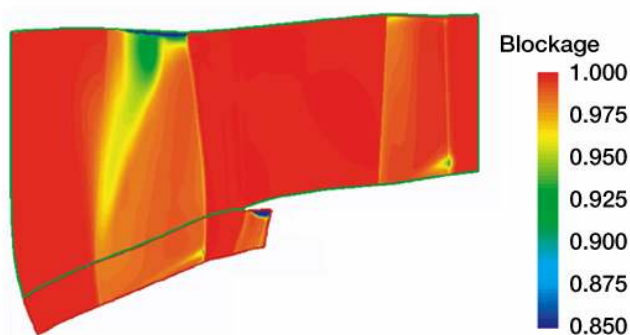


Figure 9.—Contours of blockage in the fan domain.

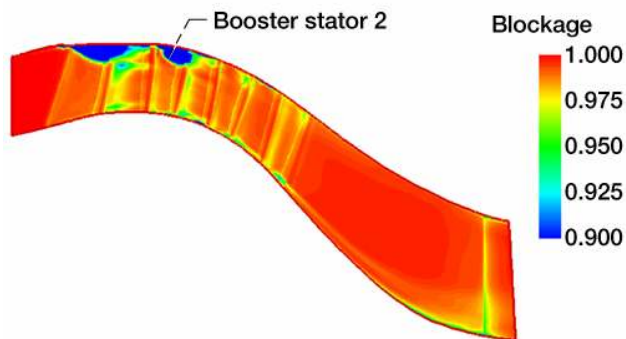


Figure 10.—Contours of blockage in the booster domain.

To the authors' knowledge, this is the first complete simulation of an entire dual-spool engine at a given point. As mentioned, there is an ongoing effort to make this simulation more consistent. These simulations present the state of the art for predicting the full engine aerodynamics. It can also be used for better component simulations, and to understand the flow fields better at realistic conditions. Blockage and the flow details it represents will be presented as one method to look at the flow fields in the turbomachinery.

Figure 9 shows contours of blockage for the fan domain that includes the fan, OGV and booster stator 1. Clearly seen is the blockage due to the shock in the fan, the tip clearance vortex, and the secondary flows at the hub for both the fan and OGV. Contours of blockage in the booster are shown in figures 10 and 11. A separation near the casing of booster stator 2 is obvious from figure 11. A radial profile of blockage and tangential flow angles just downstream of booster stator 2 are shown in figure 12. The tangential angle labeled as "derived" is based on equation (12), and the one shown as "based on momentum area average" is based on the arc tangent of the area

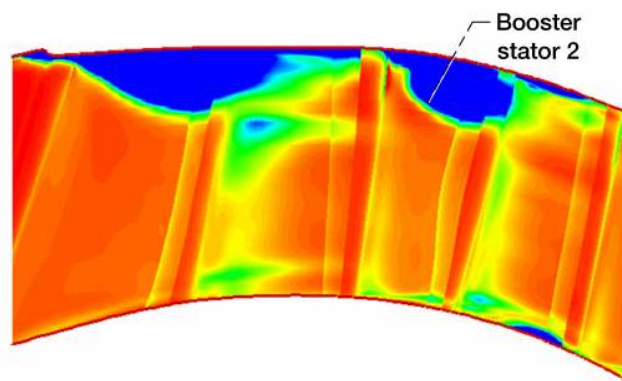


Figure 11.—Enlarged view of Figure 10 showing blockage in the front part of the booster domain.

average of the tangential and axial momentum. The difference in this angle is quite large where the blockage is large, and represents the importance of the deterministic source terms in the average passage model. Streamlines in the separated region of booster stator 2 are shown in figure 13. It is a corner separation that does not impact the loss immensely, but is important to the blockage and most likely to the stability of the machine.

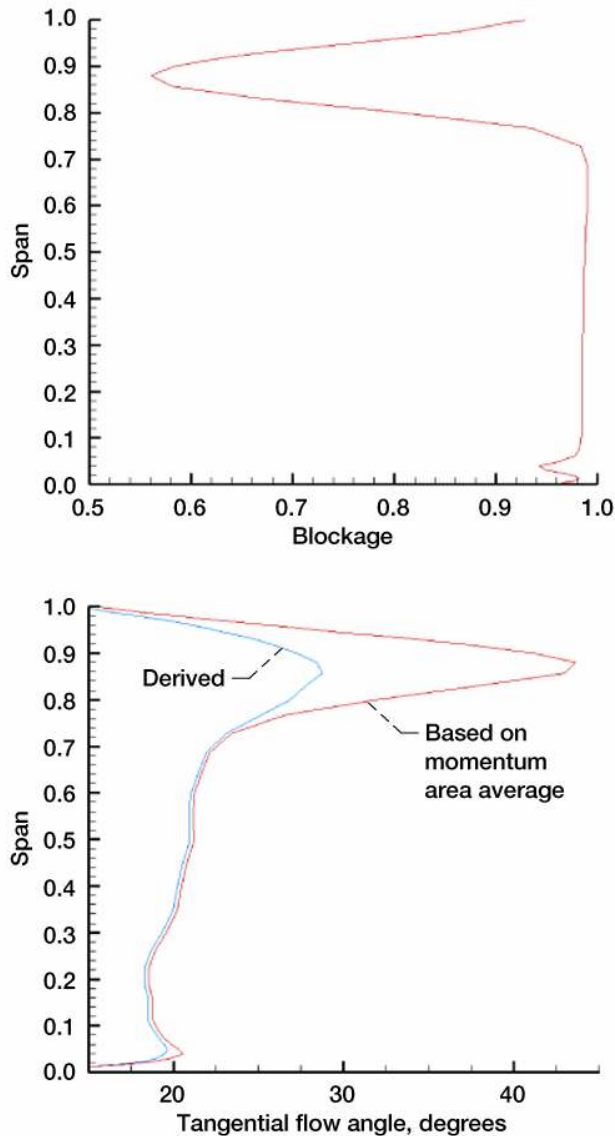


Figure 12.—Radial profiles of blockage and tangential flow angle just downstream of the booster stator 2 trailing edge. The derived angle is part of the blockage calculation.

The blockage contours for the HPC are shown in figure 14, with a zoomed region near stator 2. Observe how the level starts at 1 at the inlet and goes to mean-line value of 0.88 by stage 10. This axial blockage distribution effects the matching in a highly loaded compressor such as the GE90. Figure 15 shows the radial profiles of blockage and tangential angles similar to figure 12, but behind the trailing edge of HPC stator 2. The aero blockage has a minimum value of 0.895 at 70 percent span due to a separation on the suction surface of the stator from 50- to 90-percent span. The angles at the trailing edge are plotted in

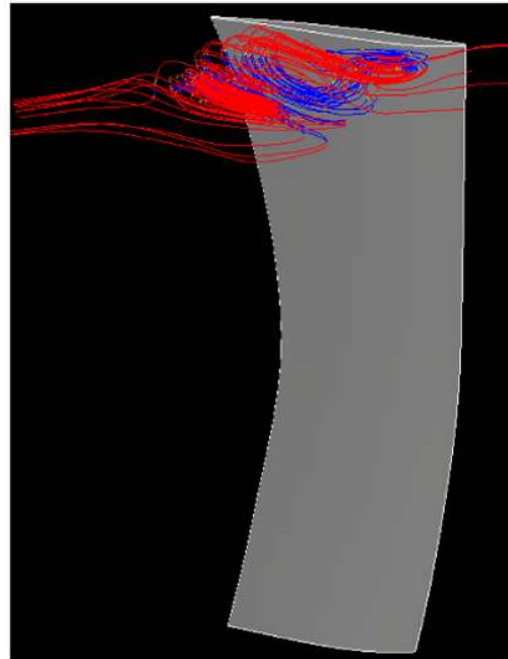


Figure 13.—Streamlines at casing of booster stator 2 showing corner separation.

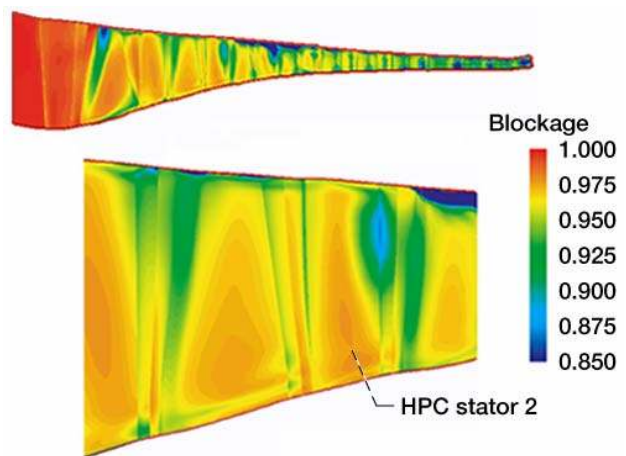


Figure 14.—Blockage contours for HPC, and zoomed region near stator 2.

figure 16 that correspond to the radial profile of angles in figure 15. The contours show underturning at the hub and casing. The separation is not very conspicuous in this plot due to the large radial exit angle variation. However, it is useful to see the extent of the tangential variation of angle.

Figure 17 shows the blockage in the HPC domain in the vicinity of rotor 6. Low values of blockage can be seen near the hub and tip of rotor 6. Figure 18 shows the cause of this blockage: a separation on the suction surface near the hub and the tip clearance vortex. Figure 19 shows

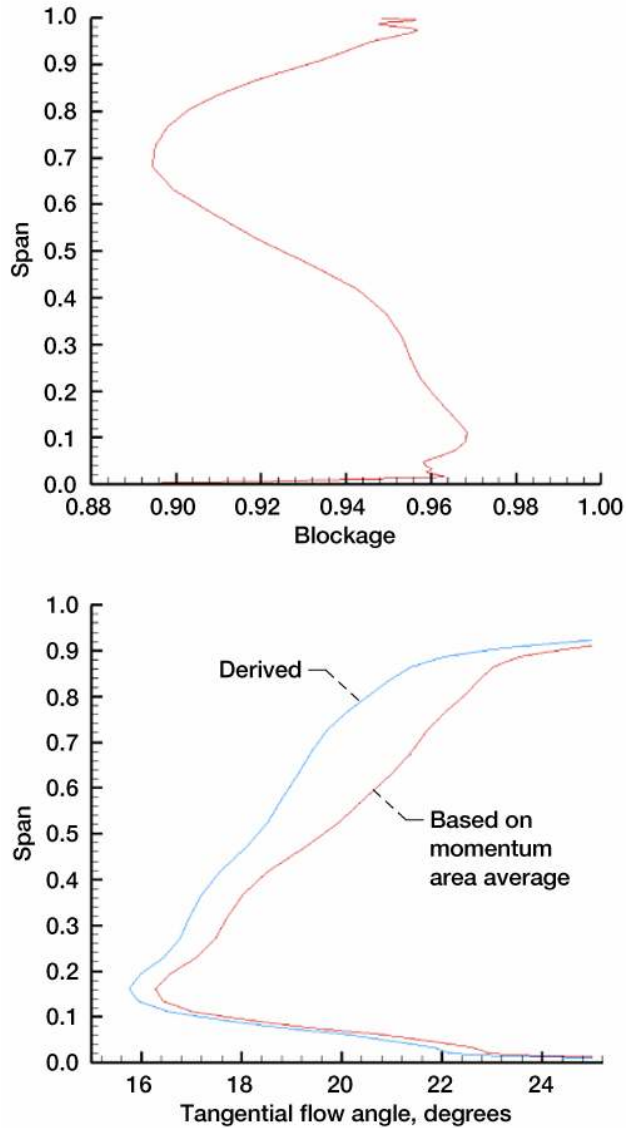


Figure 15.—Radial profiles of blockage and tangential flow angle just downstream of the HPC stator 2 trailing edge.

the radial profiles of blockage and absolute tangential flow angle. Even at midspan, where the flow is clean, the blockage has a value of 0.94. The cumulative multistage effects, through the deterministic sources have contributed to this low value. An angle difference of 2° to 3° can be seen between the blockage derived quantity and that based on the area averaged momentum.

Figures 20 and 21 show the contours of blockage below unity for the HPT and LPT, respectively. There are values above unity that exist from just upstream of the throat to downstream of the uncovered region for most of the blade rows, especially the nozzles. It is not fully understood why the blockage would be greater than one, and

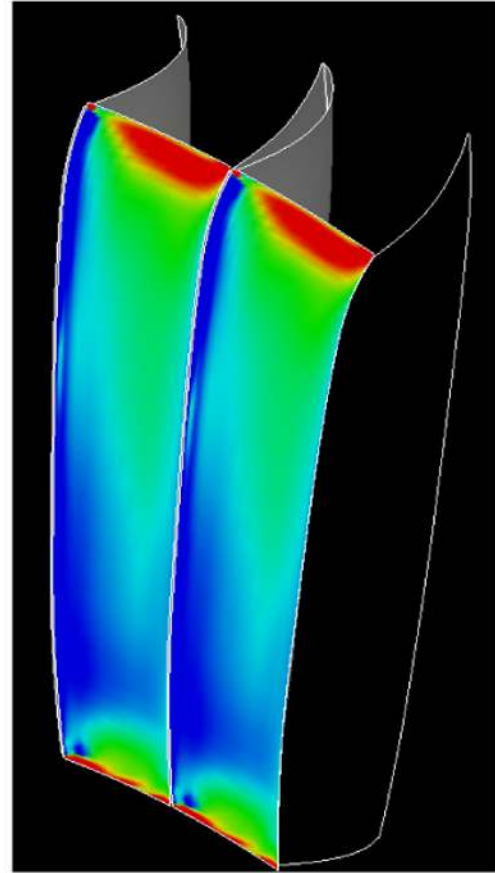


Figure 16.—Absolute flow angle at the trailing edge of stator 2 of the HPC. Angles vary from 15 (blue) to 30 (red) degrees.

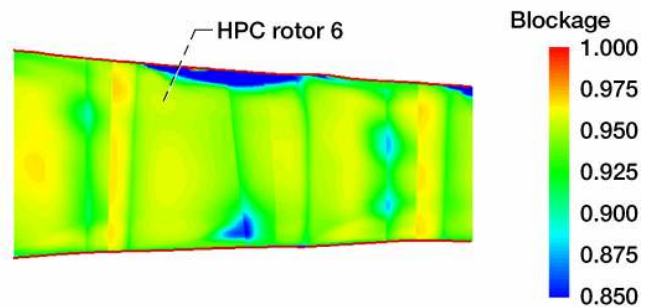


Figure 17.—Blockage contours in the HPC domain near rotor 6.

is currently being explored. It is consistent with turbine flow coefficients being greater than unity under some conditions. These contours still show areas to explore. One of these is a hub secondary flow vortex in LPT rotor 5 shown in figure 21 and through vorticity contours and streamlines in figure 22.

In highly loaded turbomachinery, blockage plays a critical role in the radial distribution of flow and being able to pass the flow, especially at high Mach

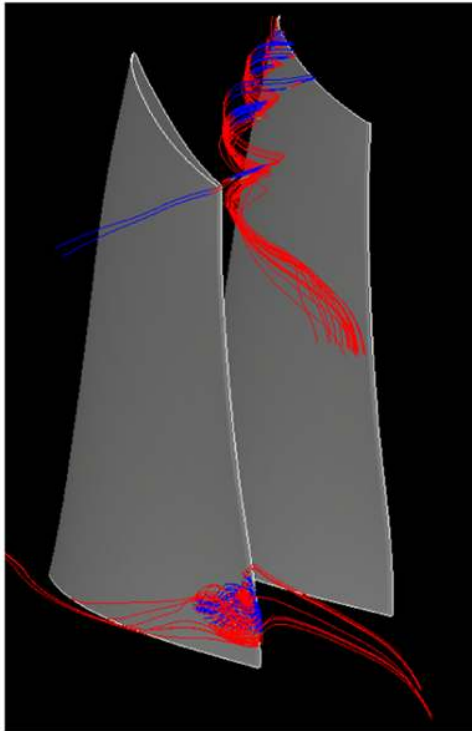


Figure 18.—Streamlines in HPC rotor 6 showing tip vortex and hub corner separation.

numbers. As demonstrated, aerodynamic blockage demonstrates the location of shocks, secondary flows, separated regions, large wakes, and multi-stage interaction effects. These multistage effects come from the deterministic sources that are part of the average passage approach. A mixing-plane approach would produce a loss, and a discontinuity at the interface, and not a blockage. The aerodynamic effect is not the same. Often a compressor rotor and stator are analyzed as isolated blade rows. It is very difficult to get the effects of blockage that are implicit in the average passage solution, except by running at a lower flow and lower speed and modifying the boundary conditions. However, this does not fully mimic the total effect of blockage since the machine runs differently at higher speeds and the variation of blockage is not uniform spanwise as shown for a few of the blade rows. Flow angles for the stator are also very difficult to get right when the level of blockage is not correct. Turbines are also affected by blockage such as turbine throat setting and turbine thrust balance. These can be predicted better when blockage is addressed in the design process.

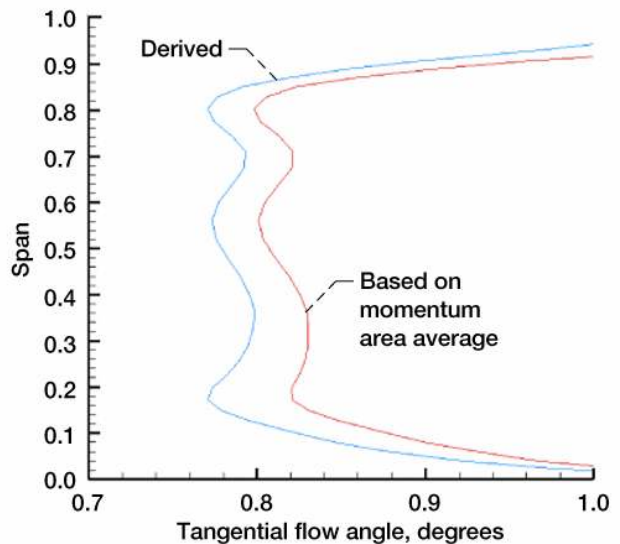
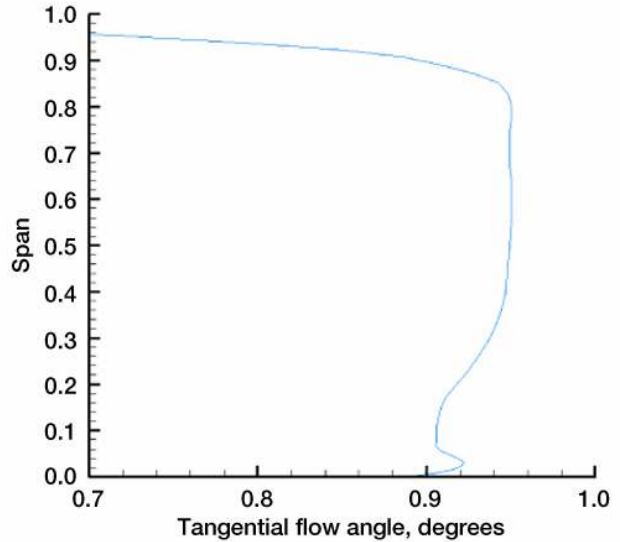


Figure 19.—Radial profiles of blockage and tangential flow angle just downstream of the HPC rotor 6 trailing edge.

Conclusions and Future Work

A successful simulation of the three-dimensional flow in the primary flow path of the GE90–94B high bypass ratio turbofan engine has been achieved. It would take less than 11 hr of wall clock time if starting from scratch through the exploitation of parallel processing. The engine simulation matches the engine thermodynamic cycle at a sea-level takeoff condition. Comparisons with the cycle are presented. Details of the turbomachinery solution using a blockage analysis have also been presented. Aerodynamic blockage

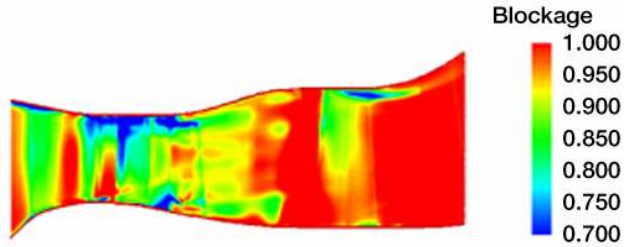


Figure 20.—Blockage contours in the HPT.

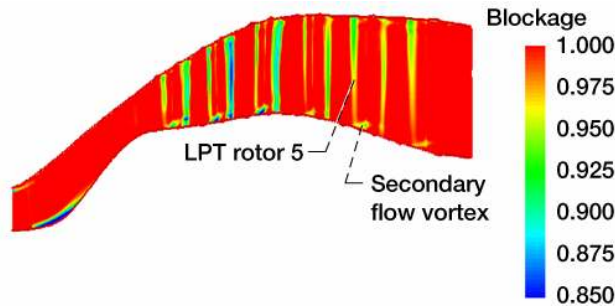


Figure 21.—Blockage contours in the LPT.

demonstrates the location of shocks, secondary flows, separated regions, large wakes, and multi-stage interaction effects.

Future work will couple the simulation to the cycle analysis using minimaps of the simulated components. The cycle will be used to balance the simulation and a front-to-back simulation will be performed. If necessary, this process will be iterated. This should eliminate any flow discrepancies between components in pressure, temperature and flow rate seen in the current simulation.

References

1. Adamczyk, J.J.; Mulac, R.A.; and Celestina, M.L.: A Model for Closing the Inviscid Form of the Average-Passage Equation System. *J. Turbomachinery*, vol. 108, 1986, pp. 180–186.
2. Adamczyk, J.J.: Aerodynamic Analysis of Multi-stage Turbomachinery Flows in Support of Aerodynamic Design. *J. Turbomachinery*, vol. 122, issue 2, 2000, pp. 189–217.
3. Ebrahimi, H.B., et al.: A Measurement Archive for Validation of the National Combustion Code. AIAA Paper 2001–0811, 2001.
4. Hunter, S.D.: Source Term Modeling of End-wall Cavity Flow Effects on Gaspath Aerodynamics in an Axial Flow Turbine. Ph.D. Thesis, University of Cincinnati, Nov. 1998.
5. Kirtley, K.R.; M.G. Turner; and S. Saeidi: An Average Passage Closure Model for General Meshes. ASME 99–GT–077, 1999.
6. Liu, N.-S.: On the Comprehensive Modeling and Simulation of Combustion Systems. AIAA Paper 2001–0805, 2001.
7. Quealy, A.: National Combustion Code Parallel Performance Enhancements. AIAA Paper 2002–3706, 2001.
8. Ryder, R.C. and McDivitt, T.: Application of the National Combustion Code Towards Industrial Gas Fired Heaters. AIAA Paper 2000–0456, 2000.
9. Shabbir, A., et al.: The Effect of Hub Leakage Flow on Two High Speed Axial Flow Compressor Rotors. ASME Paper 97–GT–346, 1997.

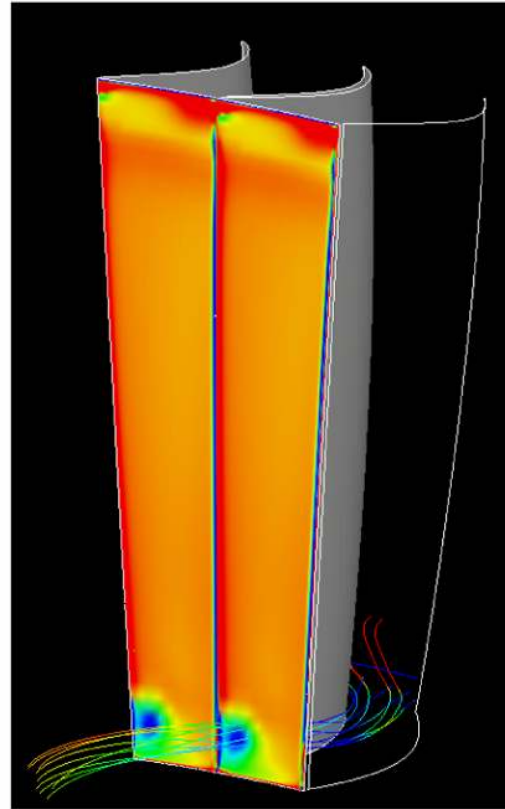


Figure 22.—Vorticity contours at the trailing edge of LPT rotor 5 showing secondary flow core.

10. Turner, M.G.: Multistage Turbine Simulations with Vortex-Blade Interaction. *J. Turbomachinery*, vol. 118, no. 4, 1996, pp. 643–653.
11. Turner, M.G., et al.: Multi-stage Simulations of the GE90 Turbine. *ASME 99-GT-98*, 1999.
12. Turner, M.G.: Full 3D Analysis of the GE90 Turbofan Primary Flowpath. *NASA/CR—2000-209951*, 2000.
13. Turner, M.G., et al.: High Fidelity 3D Turbofan Engine Simulation With Emphasis on Turbomachinery-Combustor Coupling. *AIAA-2002-3769*, 2002.

REPORT DOCUMENTATION PAGE

Form Approved
OMB No. 0704-0188

Public reporting burden for this collection of information is estimated to average 1 hour per response, including the time for reviewing instructions, searching existing data sources, gathering and maintaining the data needed, and completing and reviewing the collection of information. Send comments regarding this burden estimate or any other aspect of this collection of information, including suggestions for reducing this burden, to Washington Headquarters Services, Directorate for Information Operations and Reports, 1215 Jefferson Davis Highway, Suite 1204, Arlington, VA 22202-4302, and to the Office of Management and Budget, Paperwork Reduction Project (0704-0188), Washington, DC 20503.

1. AGENCY USE ONLY (<i>Leave blank</i>)		2. REPORT DATE March 2004	3. REPORT TYPE AND DATES COVERED Technical Memorandum	
4. TITLE AND SUBTITLE High-Fidelity Three-Dimensional Simulation of the GE90			5. FUNDING NUMBERS WBS-22-708-87-01	
6. AUTHOR(S) Mark G. Turner, Andrew Norris, and Joseph P. Veres				
7. PERFORMING ORGANIZATION NAME(S) AND ADDRESS(ES) National Aeronautics and Space Administration John H. Glenn Research Center at Lewis Field Cleveland, Ohio 44135-3191			8. PERFORMING ORGANIZATION REPORT NUMBER E-14456	
9. SPONSORING/MONITORING AGENCY NAME(S) AND ADDRESS(ES) National Aeronautics and Space Administration Washington, DC 20546-0001			10. SPONSORING/MONITORING AGENCY REPORT NUMBER NASA TM-2004-212981 AIAA-2003-3996	
11. SUPPLEMENTARY NOTES Prepared for the 16th Computational Fluid Dynamics Conference and the 33rd Fluid Dynamics Conference and Exhibit sponsored by the American Institute of Aeronautics and Astronautics, Orlando, Florida, June 23-26, 2003. Mark G. Turner, University of Cincinnati, Cincinnati, Ohio 45220-2873; Andrew Norris, Ohio Aerospace Institute, Brook Park, Ohio 44142; and Joseph P. Veres, NASA Glenn Research Center. Responsible person, Joseph P. Veres, organization code 2900, 216-433-2436.				
12a. DISTRIBUTION/AVAILABILITY STATEMENT Unclassified - Unlimited Subject Categories: 02 and 07 Available electronically at http://gltrs.grc.nasa.gov This publication is available from the NASA Center for AeroSpace Information, 301-621-0390.			12b. DISTRIBUTION CODE	
13. ABSTRACT (<i>Maximum 200 words</i>) A full-engine simulation of the three-dimensional flow in the GE90-94B high-bypass ratio turbofan engine has been achieved. It would take less than 11 hr of wall clock time if starting from scratch through the exploitation of parallel processing. The simulation of the compressor components, the cooled high-pressure turbine, and the low-pressure turbine was performed using the APNASA turbomachinery flow code. The combustor flow and chemistry were simulated using the National Combustor Code (NCC). The engine simulation matches the engine thermodynamic cycle for a sea-level takeoff condition. The simulation is started at the inlet of the fan and progresses downstream. Comparisons with the cycle point are presented. A detailed look at the blockage in the turbomachinery is presented as one measure to assess and view the solution and the multistage interaction effects.				
14. SUBJECT TERMS Turbine engines; Propulsion; System model; Computational fluid dynamics; Fan; Compressor; Turbine; Combustor; Turbomachine			15. NUMBER OF PAGES 19	
			16. PRICE CODE	
17. SECURITY CLASSIFICATION OF REPORT Unclassified	18. SECURITY CLASSIFICATION OF THIS PAGE Unclassified	19. SECURITY CLASSIFICATION OF ABSTRACT Unclassified	20. LIMITATION OF ABSTRACT	